LA-UR- 03-0368

*Approved for public release; distribution is unlimited.*

| | |
|---|---|
| *Title:* | CALCULATIONS OF THE STRUCTURE AND PROPERTIES OF RAPIDLY QUENCHED NI/ZR ALLOYS |
| *Author(s):* | F.J. CHERNE, M.I. BASKES, R.B. SCHWARZ, AND S.G. SRINIVASAN |
| *Submitted to:* | Materials Research Society's 2002 Fall Meeting, December 2-6, Boston, MA |




Form 836 (8/00)

# Calculations of the Structure and Properties of Rapidly Quenched Ni/Zr Alloys

F. J. Cherne, M. I. Baskes, R. B. Schwarz, and S. G. Srinivasan
Materials Science and Technology Division, Los Alamos National Laboratory,
Los Alamos, NM 87545-1663, U.S.A.

## ABSTRACT

Using molecular dynamics and a modified embedded atom potential developed by our group we studied the diffusivity and viscosity of molten $Ni_{1-x}Zr_x$ alloys as a function of composition, temperature, and cooling rate. Previous results indicate that these potentials represent the Ni-Zr system quite well. Liquid alloys were quenched at rates of $5 \times 10^{11}$ and $10^{12}$ K/s. For $x < 0.04$ the solidified alloys were crystalline. For higher $x$ values, the solidified alloys were amorphous. For the amorphous alloys, the composition dependence of the calculated glass transition temperature $T_g$ follows the general trend of experimental $T_g$ values. The calculated viscosity and diffusivity show systematic variation with composition. For the undercooled Ni-6 at.% Zr melt the calculated viscosity shows the Vogel-Fulcher-Tamman (VFT) behavior characteristic of a "fragile" glass.

## INTRODUCTION

In prior work [1], we used a modified embedded atom method (MEAM) to study phase stability in the nickel-zirconium system. This model predicted the stability of the observed crystalline phases quite well and the calculated shear moduli for the amorphous phases matched experiment as well. It became apparent in these calculations, however, that the potential of pure Zr needed improvement to obtain better agreement between the calculated value of the elastic constant $C_{66}$ of $NiZr_2$ and the value reported by Eshelman and Smith [2]. In the present paper we improve the atomic potentials used in the original work. We then examine the transport properties of the metallic glasses in the nickel-zirconium system.

## MEAM POTENTIAL

The MEAM formalism [3-7] is well documented in the literature and will not be described here. For nickel we employ the basic functions described in Ref. [8], with one alteration being the extension of the radial cutoff distance, $r_{cut}$, from 4.0 to 4.8 Å. This change does not affect the properties of the solid phases but ensures the conservation of energy in the liquid phases. For zirconium and for nickel-zirconium alloys we developed a new set of functions. This is done following the technique described in our prior paper [1], which addresses the aforementioned issues. The new parameters are summarized in Tables 1 and 2. Table 3 shows that these new parameters give a better fit between the calculated and measured elastic constants of $NiZr_2$ reported in the literature.

Using our new potential we calculate the enthalpy of formation for the various crystalline phases across the $Ni_{1-x}Zr_x$ composition range. In Fig. 1 we compare these formation energies to the experimental values. From this figure we see that even though the potential appears to be valid throughout the composition range, there seems to be a better agreement between the formation energies for the intermetallics on the zirconium-rich side of the phase diagram.

**Table I.** MEAM-potential parameters for Ni, Zr, and Ni-Zr used in the present work. Values listed are the cohesive energy $E_c$ (eV), the equilibrium nearest-neighbor distance $r_e$ (Å), the exponential decay factor for the universal energy function $\alpha$, the scaling factor for the embedding energy $A$, the four exponential decay factors for the atomic densities $\beta^{(l)}$, the three weighting factors for the atomic densities $t^{(l)}$, and the density scaling factor $\rho_0^a$.

| | $E_c$ | $r_e$ | $\alpha$ | A | $\beta^{(0)}$ | $\beta^{(1)}$ | $\beta^{(2)}$ | $\beta^{(3)}$ | $t^{(1)}$ | $t^{(2)}$ | $t^{(3)}$ | $\rho_0^a$ |
|---|---|---|---|---|---|---|---|---|---|---|---|---|
| Ni | 4.45 | 2.49 | 4.99 | 1.10 | 2.45 | 1.50 | 6.0 | 1.50 | 5.79 | 1.60 | 3.70 | 1.0 |
| Zr | 6.325 | 3.21 | 4.46 | 1.03 | 3.70 | 1.00 | 5.70 | 1.00 | 5.00 | 4.50 | -3.5 | 0.63 |
| NiZr | 5.868 | 2.52 | 3.999 | - | - | - | - | - | - | - | - | - |

**Table II.** Angular screening parameters for the MEAM potentials.

| | Ni-Ni-Ni | Ni-Zr-Ni | Zr-Ni-Ni | Zr-Zr-Ni | Zr-Ni-Zr | Zr-Zr-Zr |
|---|---|---|---|---|---|---|
| $C_{max}$ | 2.8 | 2.8 | 2.8 | 2.8 | 2.8 | 2.8 |
| $C_{min}$ | 0.8 | 0.5 | 0.5 | 0.9 | 0.1 | 1.2 |

**Table III.** Calculated elastic constants (GPa) for $NiZr_2$. $\mu$ is the shear modulus for a poly-crystal calculated by the Voigt average [9,10].

| | Current Work | Prior Work[1] | Experiment[2] |
|---|---|---|---|
| $C_{11}$ | 165.9 | 166.7 | 159.5 |
| $C_{12}$ | 127.8 | 114.0 | 133.7 |
| $C_{13}$ | 79.7 | 87.7 | 84.8 |
| $C_{33}$ | 141.8 | 144.7 | 146.5 |
| $C_{44}$ | 29.3 | 35.5 | 24.2 |
| $C_{66}$ | 75.0 | 83.3 | 5.62 |
| $B$ | 117.9 | 117.4 | 119.1 |
| $\mu$ | 37.2 | 43.4 | 21.6 |

[1] Reference [1].
[2] at 4.2 K, from Reference [2].

## METHOD

We used molecular dynamics (MD) to calculate quenching sequences in an isobaric-isothermal (NPT) ensemble. The MD calculations were performed on 3-dimensional periodic cells of 1500 atoms, using a time step of 1 fs. Constant temperature was maintained by using a Nosé-Hoover thermostat [11]. The Parinello-Rahman method for pressure control was used maintaining the pressure to within ±100 bar. The MD sequences were started at a temperature slightly above the melting point of the alloy. For each sequence, after thermally equilibrating the liquid state for 25 ps, the ensemble was cooled at 10 K increments, being held at each step in temperature for the length of time needed to achieve the desired cooling rate. For example, for a $10^{12}$ K/s cooling rate, the holding time at each step was 10 ps. The quench rates studied here were $10^{12}$ K/s and 5 x $10^{11}$ K/s. These calculations were used to generate plots of the average

volume and the average energy versus temperature. From these plots we determined the transition temperatures $T_g$ to the glassy state, or $T_x$ to the crystalline state.

We also determined the diffusivity of Ni and Zr atoms in the alloy from their mean-square displacements and we calculated the viscosity coefficient using the method described by Holian [12]. This method uses standard 3-dimensional periodic boundary conditions and imposes a mass-average velocity, $u_p$ in one half of the sample, and the velocity $-u_p$ in the other half. This formalism results in a relationship between the kinematic viscosity $\upsilon$ and the driving force to maintain the given velocity, which is:

$$\nu = -\frac{\bar{g}^{SS} w^2}{\pi^2 u_p} \tag{2}$$

where $\bar{g}^{SS}$ is the steady-state time-averaged driving acceleration, and $w$ is the half width of the periodic box. The resulting shear viscosity is calculated by extrapolating the calculated viscosity to zero shear rate. For these simulations, we applied a range of shear rates from $10^{10}$ to $10^{11}$ $s^{-1}$. Complete details of this procedure are found in reference [12].

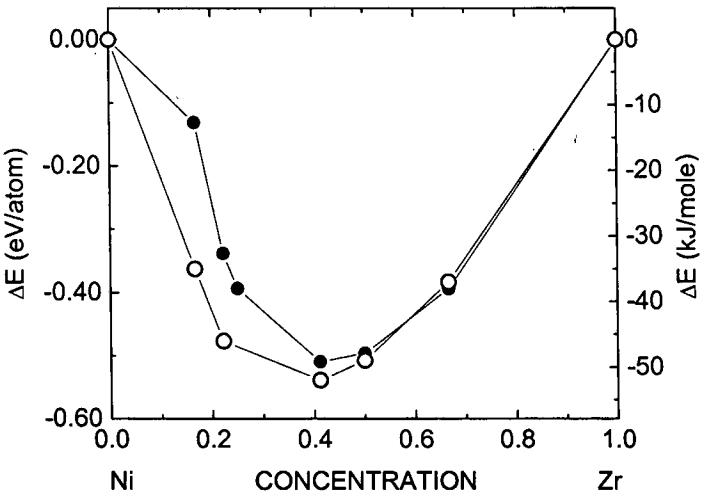


**Figure 1.** Enthalpy of formation, $\Delta E$ for the crystalline phases in the Ni-Zr system. The solid symbols are the calculated $\Delta E$ for the crystalline phases at 0 K whereas the open symbols represent the experimental heats of formation at 298 K.

## RESULTS AND DISCUSSION

Figures 2(a) and 2(b) show the average energies of the Ni-Zr melts while being quenched at $10^{12}$ K/s and 5 x $10^{11}$ K/s. The Ni-rich alloys show abrupt drops in energy at constant temperature, characteristic of first-order phase transitions. Even at these high cooling rates, pure Ni and the Ni-rich melts crystallize on cooling. Crystallization was verified by examining the atom positions. The energy-temperature curves for higher Zr concentration show no abrupt isothermal decrease in energy. These curves show instead slight changes in slope, and the

temperature where these change occur were identified as the glass transition temperatures. Notice in these figures that the alloys containing 3 and 4 at.% Zr crystallize at the cooling rate of 5 x $10^{11}$ K/s but are kinetically trapped in the glassy state at the faster cooling rate of $10^{12}$ K/s.

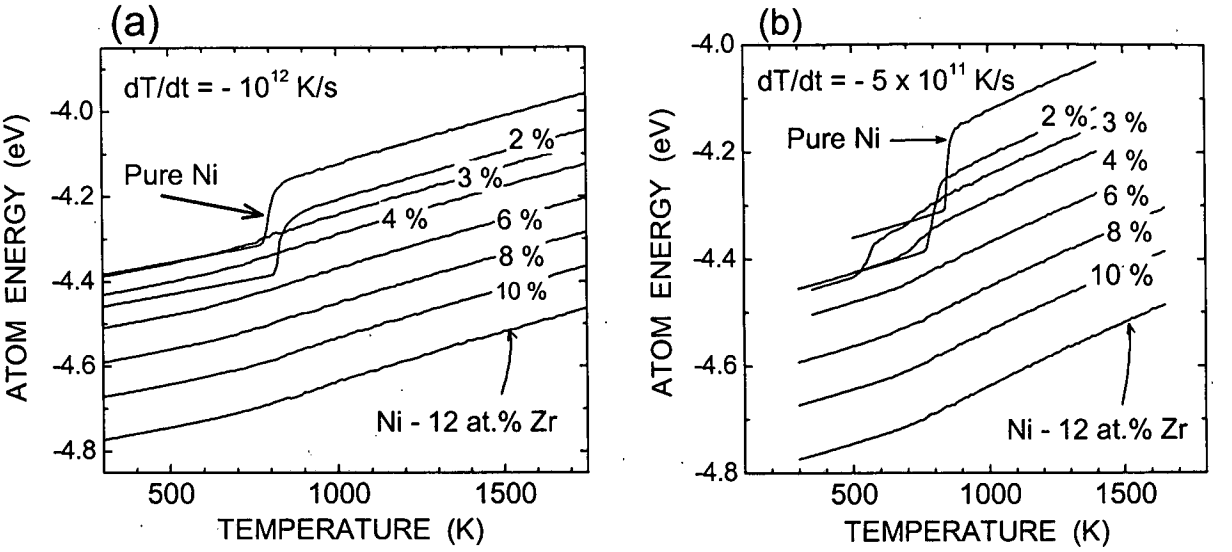


**Figure 2. Average** energy versus temperature during the cooling of Ni-Zr melts at rates of $10^{12}$ K/s (a) and 5 x $10^{11}$ K/s (b).

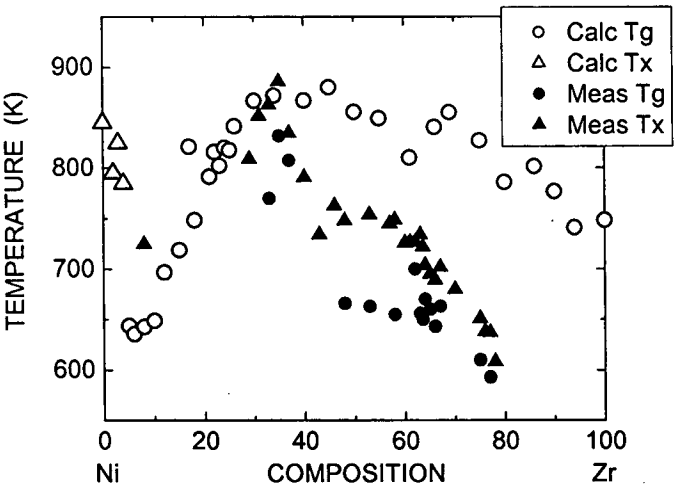


**Figure 3.** MD simulation results for $T_X$ (open triangles) and $T_g$ (open circles) obtained at the cooling rate of 5 x $10^{11}$ K/s. The filled triangles and circles are experimental $T_X$ and $T_g$ values measured while heating glass prepared at a cooling rate of approximately $10^6$ K/s (from Ref. [13]).

Figure 3 shows $T_g$ and $T_X$ values deduced from simulations at the *cooling* rate of 5 x $10^{11}$ K/s. Our MD results for a cooling rate of $10^{12}$ K/s are quite similar to those shown. We do not have calculated $T_g$ and $T_X$ values for *heating* runs at rates of $10^6$ K/s. Therefore, a comparison of our calculated $T_g$ and $T_X$ values with the available experimental data is meaningless. However, the $T_g$ values measured on heating glassy alloys prepared at quenching rates on the

order of $10^6$ K/s (solid circles) are significantly lower than our simulation results, as expected on the account of the large difference in quenching rates.

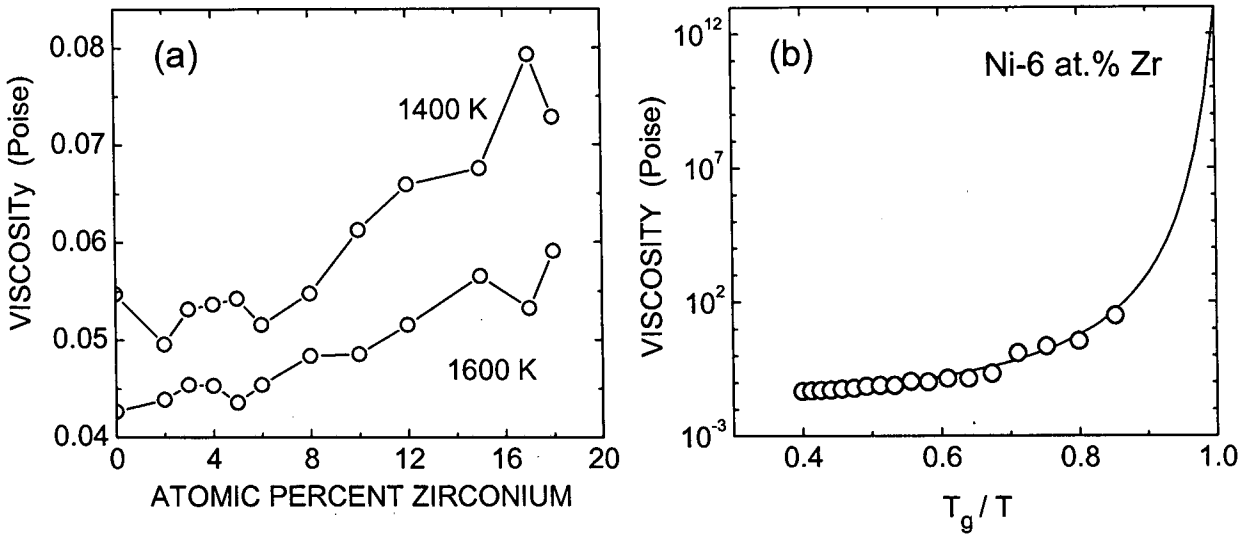


Figure 4. (a) Viscosity of $Ni_{1-x}Zr_x$ melt as a function of composition. (b) Viscosity of Ni-6 at.% Zr as a function of inverse temperature. The quenching rate for all the alloys was $10^{12}$ K/s. The solid curve in Fig. 4(b) is the VFT fit to the calculated viscosity.

Figure 4(a) shows the viscosity of $Ni_{1-x}Zr_x$ melt as a function of composition at temperatures of 1400 and 1600 K. Over this limited composition range, the viscosity increases monotonically with increasing Zr content. Figure 4(b) shows the viscosity of Ni-6 at.% Zr melt as a function of $T_g$ / T, using the $T_g$ value of 640 K deduced from Fig. 3. The solid curve in Fig. 4(b) is a fit to the data using the Vogel-Fulcher-Tamman (VFT) expression, $\eta = \eta_o \exp(D\, T_O/(T - T_O))$, using the values $\eta_o = 0.012$ Poise, $D = 2$, and $T_O = 605$ K. The fitted value for $\eta_o$ is within a factor of two from the value predicted by Nemilov [14], $\eta_o = N_A\, h\, /\, V = 0.0057$ Poise, where $N_A$ is Avogadro's number, $h$ is Plank's constant, and $V$ is the alloy's molar volume. The fitted value $D = 2$ is characteristic of a "fragile" glass, which is expected for this alloy melt because it has only 6 at.% solute. For a good glass former, such as $Zr_{41}Ti_{13}Cu_{12}Ni_{10}Be_{22}$, $D \approx 20$ [15]. For a very "strong" glass, such as $SiO_2$, $D \approx 100$. The fitted value of $T_O$ is quite reasonable since experience has shown that for fragile glasses $T_O$ is typically 30 to 50 K lower than $T_g$.

Figure 5 shows the compositional dependence of the diffusivity of Ni and Zr atoms in Ni-6 at.% Zr melt at T = 1100 K and 1400 K. The calculated diffusivity for Ni is greater than that of Zr as we would expect because zirconium atoms are larger than nickel atoms. The diffusivities of both Ni and Zr show a weak minimum at intermediate concentrations.

## CONCLUSIONS.

We have demonstrated that molecular dynamics simulations based on Ni-Zr potentials developed with the MEAM formalism can realistically describe rapid solidification. The predicted formation enthalpies of the various intermetallic phases in the Ni-Zr system are in reasonable agreement with experiment. A transition between crystallization and amorphization is predicted as a function of quench rate and alloy composition. Predicted glass transition temperatures are in reasonable agreement with experiment. Calculated values of the viscosity of

Ni-6 at.% Zr show this alloy is a "fragile" glass former. The viscosity increases rapidly with temperature as the glass transition temperature is approached, in agreement with the VFT behavior.

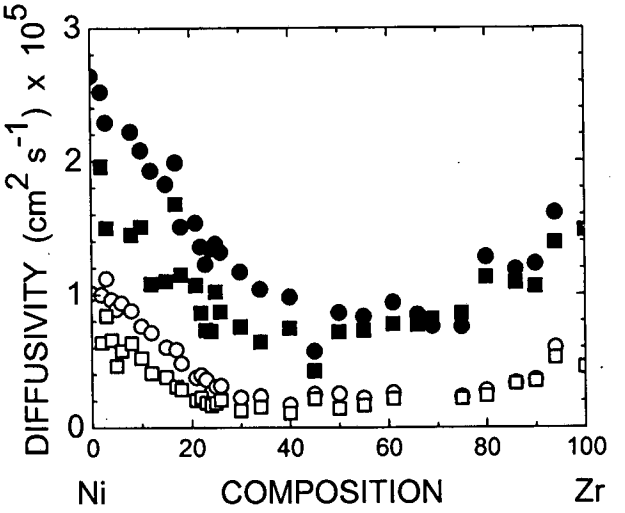


**Figure 5.** Diffusivity of nickel (circle) and zirconium (square) at quench rate of $10^{12}$ K/s as a function of composition at 1400 K (filled) and 1100 K (open).


## ACKNOWLEDGEMENTS

This research was supported by the US Department of Energy, office of Basic Energy Sciences.


## REFERENCES


1. F. J. Cherne, M. I. Baskes, and R. B. Schwarz, accepted for publication in *J. of Non-Crystalline Solids.*
2. F. R. Eshelman, and J. F. Smith, *J. Appl. Phys.* **46,** 5080 (1975).
3. M. I. Baskes, *Phys. Rev. B* **50,** 795 (1994).
4. M. I. Baskes, *Mater. Sci. and Eng.* A, **A261,** 165 (1999).
5. M. S. Daw and M. I. Baskes, *Phys. Rev. B* **29,** 6443 (1984).
6. M. S. Daw, S. M. Foiles, and M. I. Baskes, *Mater. Sci. Rep.* **9,** 251 (1993).
7. M. I. Baskes and R. A. Johnson, *Modelling Simul. Mater. Sci. Eng.* **2,** 147 (1994).
8. M. I. Baskes, *Mater. Chem. and Phys.,* **50,** 152 (1997).
9. G. Simmons and H. Wang, *Single Crystal Elastic Constants and Calculated Aggregate Properties: A Handbook,* (The M.I.T Press, Cambridge, MA, 1971).
10. W. Voigt, *Lehrbuch der Krystallphysik,* (B. G. Teubner, Leipzig, 1928).
11. S. Nosé, *Prog. Theor. Phys. Suppl.*, **103,** 1 (1991).
12. B. L. Holian, *J. Chem. Phys.* **117,** 1173 (2002).
13. K.H.J. Buschow, *J. Phys. F: Met. Phys.* **14,** 593 (1984).
14. S. V. Nemilov, *Glass Physics and Chemistry* **21,** 91 (1995).
15. R. Busch, A. Masuhr, E. Bakker, and W. L. Johnson, *Mater. Sci. Forum* **269-272,** 547 (1998).